 FDMP, vol.8, no.1, pp.107-128, 2011

Electrically Heated Composite Leading Edges for Aircraft Anti-Icing Applications

F. De Rosa[1] **and A. Esposito**[1]

Abstract: An investigation was conducted to evaluate the feasibility and the performance of an electrically heated composite leading edge for aircraft anti-icing applications. A prototype was designed, manufactured and equipped with a High Temperature composite leading edge with embedded Ni alloy resistance fed by a DC power supply unit. Running wet and fully evaporative functional modes have been verified both analytically and experimentally with reasonable agreement. A room temperature thermal endurance test has been run for 10^4 cycles aiming to preliminary verify the integrity of the composite laminate after the imposed thermal stress. The EHCLE system (Electrical Heated Composite Leading Edge) showed an enormous potential which justify the need for future development in a larger scale under more severe icing condition for a final assessment about the applicability to real aircraft.

Keywords: Anti-icing, High Temperature Composite, Ice Protection System

Acronyms

CFRP: Carbon Fiber Reinforced Plastic
EHCLE: Electrically Heated Composite Leading Edge
FE: Fully Evaporative
FM: Functional Mode
HT: High Temperature
IFF: Icing Flow Facility
IPS: Icing Protection System
ITC: Icing Test Condition
LE: Leading Edge
LWC: Liquid Water Content
MVD: Median Volume Diameter
RT: Room Temperature (in the present work RT conditions always refer

[1] University of Naples, Naples, Italy

to 20˚C)
RW: Running Wet
TET: Thermal Endurance Test

1 Introduction

The massive introduction of CFRP materials in aircraft structures has generated the need to design and develop IPSs able to perform within composite structures which, for the limited maximum continuous service temperature of classical epoxy resins, has been for years a challenging task. Recent development of High Temperature polymers gave the possibility to reconsider the application of thermal IPSs to composite structure by reaching maximum continuous service temperatures up to 200[˚C] without significant degradation of structural properties, whilst for classical epoxy composites it was limited to around 85[˚C]. The research about low power IPSs has progressed enormously in recent years but few papers have been published about CFRP applications (see Bragg et alii 2002, Botura at alii 2006). An Electrothermal IPS is capable of either de-icing or anti-icing functionality by empowering electrical resistances which heat up the leading edge skin melting the accreted ice or preventing ice to accrete. Resistance can be bonded to the inner surface of the LE skin (metallic or composite) or embedded directly into the matrix of a composite LE (see Ross et alii, 1991). This last system, using a suitable matrix, can be lifetime reliable provided that operating temperatures will never exceed the allowed limits. The current work is an attempt to preliminary design, assemble and test a thermal IPS, named EHCLE, integrated within an HT composite structure. The IPS was built up embedding an electrical resistance within a composite leading edge skin laminate resulting in a final product which is “structure” and “system” at same time for the benefit of both. For technological reasons directly linked to the scale of the tested prototype a uniformly distributed single-path resistance was adopted leaving to future developments the possibility to investigate finer solutions using tailored multi-path resistances. The paper is focussing to the thermal performance of a scaled model against severe icing conditions and preliminarily evaluates its capabilities to reach “Running Wet” and “Fully Evaporative” functional modes. The great advantage of the investigated EHCLE system is weight and energy saving together with the possibility to de-ice any exposed surface by-passing almost all structural obstacles which are normally limiting Air-bleed and Pneumatic IPSs increasing the overall safety.

2 EHCLE Prototype Design and Analysis

The EHCLE system (see Fig. 1) was preliminarily designed by means of analytical methods, accounting for material data as declared by the material supplier and using a linear theory for steady and unsteady heat transfer. A semi-empirical method has been developed to account for accretion, melting and evaporation of ice on the basis of existing literature, see (Henry,1992), in first instance afterwards corrected on the basis of the preliminary experimental results. The thickness-wise position of the resistance is one of the major parameters within the EHCLE preliminary layout which was defined to respond to several needs imposed by the composite manufacturing processes and accounting for the overall dimension of the available icing tunnel. The airfoil type and size was chosen to maximize the uniformity and stability of the icing flow in relation to the IFF resulting in a 34[mm] thick, 283 [mm] long and 118 [mm] wide NACA0012 airfoil. For the purpose of the present work the airfoil geometry plays anyway a secondary role because no aerodynamic investigations have been performed focussing only the thermal behaviour. The thickness of the leading edge laminate, ranging 2.5 to 3.0 [mm], was chosen only to respond to the formability requirements of the laminate within the ceramic tool regardless of the basic structural needs. The laminate thickness can, in fact, be increased on the inner side, where the temperature gradient is negligible, as much as structurally needed without significant losses for the system efficiency which is driven only by the distance of the resistance from the outer surface. The resistance has been therefore positioned after the first 3 plies of carbon either to reduce the waviness induced by the resistance on the outer surface either to guarantee a minimum thickness on the outer surface to be more compliant with static and impact requirements. The layup has been built up according to basic principles of symmetry and balance and the glass plies have been introduced either to improve the adhesion around the resistance, thanks to the high formability and reduced thickness, either to guarantee the electrical insulation with respect to the conductive carbon and also to avoid galvanic corrosion between carbon and Ni alloy. The layup is schematically shown within the scheme in Fig. 3. The chordwise extension of the resistance has been set accounting for water particle impingement, erosion zone limit and structural limitations and the thermal load cases have been defined to cope from “running wet” up to “fully evaporative” functionalities.

As verified by the analytical model, the key design parameters for such heating element are the “filling factor” $\boldsymbol{K_F}$=$\boldsymbol{A_{HE}/A_D}$, defined as the ratio between total frontal area of the resistance $\boldsymbol{A_{HE}}$ and the total de-iced area $\boldsymbol{A_D}$, and the spanwise distance $\boldsymbol{W_B}$ as shown in Fig. 3. These two parameters are heavily influencing the “power density” $\boldsymbol{Q_J}$ and the “reaction time” of the system, $\boldsymbol{t_R}$, defined as the time needed by the temperature to reach a equilibrium uniform value on the external surface.

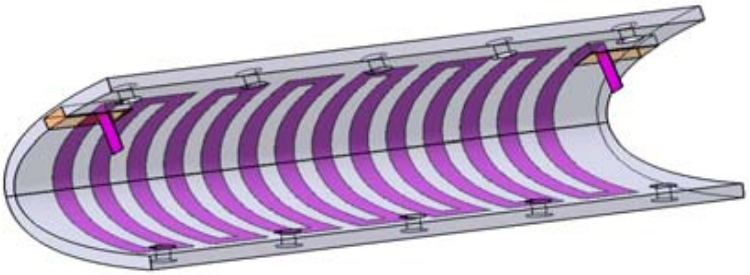

Figure 1: Electrically Heated Composite Leading Edge

The wider W_B is, the longer the reaction time $t_R$will be but, in the end, this relation breaks down at a certain value of W_B when the external surface temperature does not reach an equilibrium at all leaving on the surface different temperature zones.

Figure 2: EHCLE typical spanwise section

The analytical model has been built up taking a spanwise section and considering only one of the elementary constituents as shown is Figs. 2 and 3. Within this scheme, h_{EXT} [W m^{-2} °C^{-1}] is the convection coefficient on the external surface due to the icing flow including air and water contributions, h_{INT} [W m^{-2} °C^{-1}] is the convection coefficient on the internal surface due to natural convection in air, T_{ES} [°C] is the LE external surface temperature, T_{HE} [°C] is the heating element temperature, T_{IS} [°C] is the LE internal surface temperature, T_{EXT} [°C] is the external flow total temperature, T_{INT} is the air temperature within the LE inner cavity [°C], Q_J [Wm^{-2}] is the electrical power density averaged over A_D, Q_1[W m^{-2}] is part of Q_J which is transferred to the leading edge external environment, Q_2[W m^{-2}]is part of Q_J which is transferred to the leading edge internal environment. Power densities Q_1 and Q_2 are proportional to the heat exchanged on each side and therefore, assuming negligible losses, they are linked by the relation:

$$Q_J = Q_1 + Q_2 \tag{1}$$

Eq. (1) is indirectly defining the efficiency of the system:

$$E_{EHCLE} = Q_1/Q_J \tag{2}$$

The global heat exchange analytical model has been therefore built up using an electrical equivalent model where the governing equation can be written as:

$$P_T = \Delta V I = I^2 R_{HE} \tag{3}$$

Within Eq. (3), ΔV [V] is the applied DC voltage, I [A] is the current, P_T[W] is the total supplied power, R_{HE} [Ω] is the total resistance of the heating element.

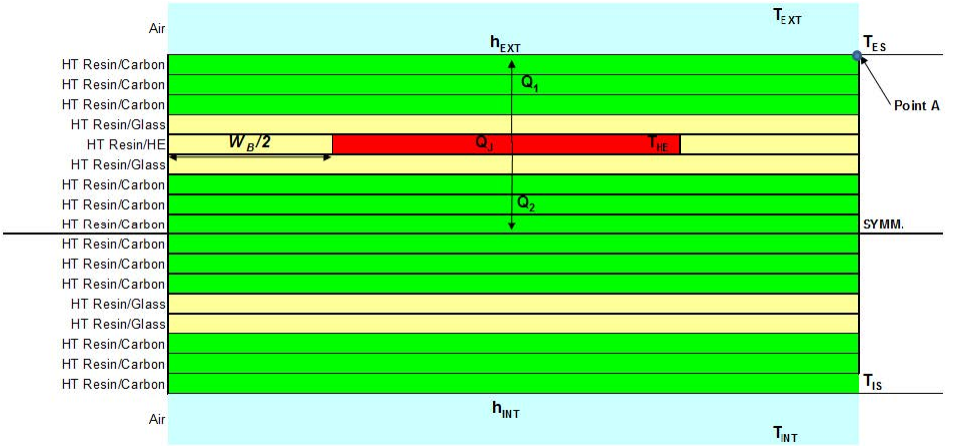

Figure 3: EHCLE elementary constituent scheme

From the previous relation we obtain the average power density as $Q_J = P_T / A_D$. The results of the analytical model are summarized in the Tab. 1 and Fig. 4. All simulations have been made at T_{EXT} = -20[°C], Mach number M=0.2 and liquid water content ***LWC=0.6*** [g m^{-3}] (see ITC5 in Tab. 3) with exception of functional modes identified by codes FM13, FM14 and FM15 which are DRY cases with ***LWC=0***. To preliminarily evaluate the reaction time t_R, an unsteady analytical model has been built up using the Lumped Capacitance Method (***Bi***<0.1) and the Heisler charts (***Bi***>0.1), see Cenghel Y.A., 2003, assuming that the system is switched-ON before any ice has accreted on the leading edge surface with an instantaneous empowering of the resistance from zero to the target value of P_T whilst for the experimental icing campaign the power was increased through a linear ramp from zero to the programmed value of P_T at a rate of 3 to 4 [W s^{-1}] to avoid dangerous peaks. In order to be more conservative the unsteady temperature calculation has been performed in the "worst case" location which is represented by the “point A” in Fig. 3. For the FE case, t_R was in the range of 4 to 5[s].

Design Param.		Functional Modes								
		FM17	FM1 FE	FM16	FM2	FM3	FM4	FM5	FM6	FM7
ΔV	[V]	18,7	17,7	17,5	17,0	16,3	15,7	15,0	14,3	13,6
I	[A]	8,52	8,09	7,97	7,78	7,46	7,15	6,84	6,53	6,22
P_T	[W]	159	143	139	132	122	112	102	93	85
Q_J	[kW m^{-2}]	30,0	27,0	26,2	25,0	23,0	21,1	19,3	17,6	16,0
Re	-	125000	130000	131000	134000	137000	140000	143000	145000	147000
T_{ES}	[°C]	80	69	66	60	52	45	39	34	29

Design Param.		Functional Modes								
		FM8	FM9	FM10	FM11	FM12 RW	FM13 DRY-RW	FM14 DRY	FM15 DRY-FE	-
ΔV	[V]	12,9	12,2	11,6	10,0	8,7	7,6	10,5	13,5	-
I	[A]	5,91	5,60	5,28	4,57	3,98	3,47	4,80	6,15	-
P_T	[W]	76	69	61	46	35	26	50	83	-
Q_J	[kW m^{-2}]	14,4	12,9	11,5	8,6	6,5	5,0	9,5	15,6	-
Re	-	149000	151000	152000	154000	156000	156000	143000	130000	-
T_{ES}	[°C]	24	20	17	12	10	10	40	70	-

Table 1: EHCLE Functional Modes calculated analytically

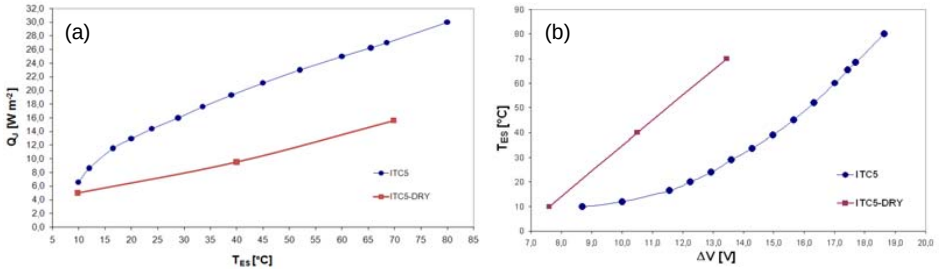

Figure 4: Power density as function of the External Surface Temperature (a); External Surface Temperature as function of the supplied voltage (b)

2.1 A critical point: Connecting the Heating Element to the Power Supply

The physical connection of the heating element to the electrical wirings has showed to be a serious technological challenge. A welded connection at laminate level would keep the heating element continuously cooled by the external flow but it would be not reliable and reparable. A mechanical connection would be more effective in real applications but to achieve the connection the resistance should be bent towards the leading edge cavity and get connected to the large cross section copper wiring through an electrical union but, once it is bent, it loses the contact with laminate and being not cooled anymore its temperature is rising up quickly. It was then necessary to get the resistance connected to the union itself as close as

possible to the laminate and this has been possible through a miniaturized union which reduced the exposed part of the resistance to about 3[mm]. The temperature of the two exposed portions of resistance (IN and OUT) have been monitored during the whole test campaign and, for the FE case, when the resistance was working at an average temperature $\boldsymbol{T}_{HE}$=105 [°C] it has shown a maximum final temperature of 140[°C].

3 EHCLE Prototypes and coupon Manufacturing

Three articles have been manufactured, two composite leading edges, EHCLE1 and ECHLE2, see Fig. 7 (a), and one flat coupon, see Fig. 7 (b), using the same material and processes. The EHCLE1 has been used for the icing test campaign, the EHCLE2 has been kept as spare and the flat coupon has been used for TET and micrographic inspections.

3.1 Materials, Processes and painting systems

The raw materials were selected on the basis of their properties and their processability accounting for market availability and budget.

The High Temperature resin choice has been by far the most critical decision made in the project. A modified epoxy resin type *Epoxy/Bisphenol-A/Epichlorhydrin* was chosen, showing the best thermal properties and by far the easiest processability.

The selected carbon fabric has been a 6K twill 200[g m^{-2}] areal weight and average cured thickness of 0.193[mm]. For cutting and handling of the dry layup the carbon sheet was bindered with HT resin applied in a quantity equivalent to around 2% of the final resin amount needed for the complete manufacturing.

The glass fabric adopted was an 80 [g m^{-2}] woven fabric which is commonly used for galvanic corrosion in aerospace composite structures.

The Heating Element material was selected according to two basic needs: electrical resistivity, to guarantee the max heating for the assigned available electrical power, and CTE (Coefficient of Thermal Expansion) very close to the composite laminate one, to avoid dangerous internal static stresses. For these reasons the Ni80Cr20 alloy was chosen and the resistance was crafted out of a 0.12[mm] sheet and finished from average roughness 0.8[μm] Ra up to 1.6 to 3.2[μm] Ra to improve the adhesion of the HT resin.

The main body was NC crafted out of oak wood plate. It was dried, impregnated with epoxy resin, cured at room temperature for one day and finished by hand to the target tolerance, which was set as 1% of the airfoil maximum thickness, to the nominal loft. All carbon plies were cut from a bindered fabric by precision hand scissors using a template with an overall precision of $\pm$0.5 [mm]. The plies

were laid up in a ceramic tooling with interposition of resin layers according to the calculated amount per ply with an over-resin of 20 to 25% to guarantee the best laminate quality. Ply positioning within the laminate wet layup was affected by an accuracy of ± 1 [mm]. Basic auxiliary materials used for moulding purposes like peel ply, release film, bleeder, breather fabric, vacuum bag and release agent have been selected among those qualified for aerospace applications, they are non-contaminant and approved for safety. The curing cycle, which has been performed in oven with operating range 0 to 350 [°C] and accuracy of $\pm 1\%$, is reported in Fig. 5(a). Pressure on the laminate was applied through vacuum bagging with final inside-bag pressure of 20[Torr]. The post-curing cycle, which has been performed in the same oven after complete cooling to RT of the cured articles previously demoulded and clean from any trace of auxiliary materials, is reported in Fig. 5(b).

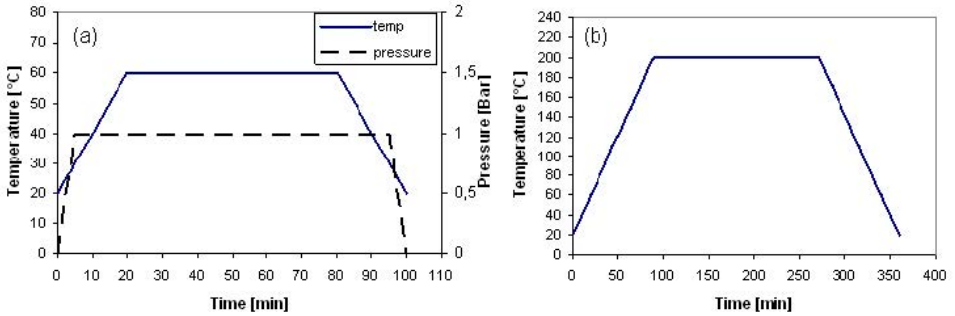

Figure 5: EHCLE Prototype curing cycle (a) and post-curing cycle (b)

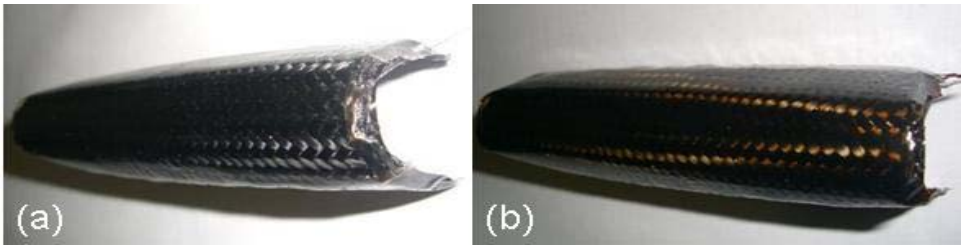

Figure 6: EHCLE Prototype after curing (a) and post-curing (b) cycles

The resin has a light yellow appearance after low temperature curing cycle and a light brown appearance after high temperature post-curing cycle as shown in Figs. 6(a) and 6(b) respectively.

The prototype main body was finished using Low-Volatile-Oxide-Content Polyurethane coating, qualified for aerospace applications within the temperature range -55 to 150 [°C], applied by spraying at RT and cured for 6[h] at RT. The final main body coating thickness was ranging 75 to 100 [μm]. The external surface of the EHCLE system was finished by HT Silicon coating applied by spraying in controlled atmosphere chamber at RT, dried in the same chamber for 4[h] and cured in oven at 150[°C] for 1.5 [h] with heat up and cool down rates of 5[°C min^{-1}]. The EHCLE system final coating thickness was ranging 30 to 40 [μm].

3.2 EHCLE laminate Fiber Volume Fraction

The Fiber Volume Fraction (see Tab. 2) has been calculated measuring all material and process parameters assuming negligible volatile contents. The weight difference between cured and post-cured articles was found to be negligible.

Measured parameter		**EHCLE1**	**EHCLE2**	**EHCLE Coupon**
Dry laminate weight	[g]	39,0	41,3	5,4
Total resin weight	[g]	29,2	29,4	3,9
Resin absorbed by absorbent fabric	[g]	6,3	5,9	0,9
Heating Element weight	[g]	2,5	2,5	0,4
Weight after postcuring	[g]	64,4	67,3	8,8
Weight after postcuring HE nett	[g]	61,9	64,8	8,4
Fiber Volume Fraction		63%	64%	64%

Table 2: Manufacturing Summary Report and Fiber Volume Fraction

3.3 EHCLE system demoulding and machining

All articles have been demoulded at RT after the curing cycle, post-cured, cooled to RT and then machined to final dimensions. The machining of the EHCLE1 produced 5 items, see Fig. 7(a): the Leading Edge to final dimensions used for icing test and Samples 1 to 4 used for micrographic inspection. The machining of the coupon, see Fig. 7(b) produced the TET coupon and Samples 5 to 7 used for micrographic inspection.

3.4 Micrographic Inspection

The micrographic inspection was performed using a microscope VISION SX45. A first inspection was performed on Samples 1 to 7 to check the overall quality of the laminate establishing an overall porosity correlation. A second micrographic

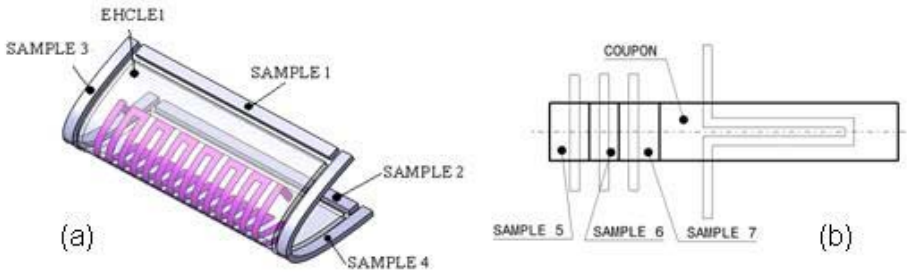

Figure 7: EHCLE1 (a) and Coupon (b) layout

inspection was performed to compare unstressed samples to those cut from the stressed coupon after TET. The porosity of the laminate obtained from the 15 examined sections ranged 0 to 2.8% with an average total porosity of 1.9%.

3.5 Prototypes dimensional control

The dimensional check of the NACA0012 assembled prototype was performed by laser scanning the airfoil half-thickness normally to chord plane. The measurements, made after finishing and painting in the assembled configuration, were taken three times to provide a valid average. The maximum spanwise deviation to the nominal loft was ± 0.5 [mm] for the main body and ± 0.3 [mm] for the composite leading edge which showed the largest deviations concentrated at the top and the bottom edges confirming the tendency of the laminate to spring-in in those locations.

3.6 EHCLE prototype assembly and instrumentation

The tested prototype is made basically of two components, the composite leading edge EHCLE1 (10% of chord length) and the main body (90% of chord length) assembled by means of screwed spanwise joints (see Fig. 8).

The prototype was equipped with 8 T-type thermocouples: TC1, dedicated to $\boldsymbol{T}_{HE}$ in the stagnation point and cemented to the heating element from the inner side in the middle of the span length, TC2, dedicated to $\boldsymbol{T}_{ES}$ in the stagnation point and cemented into the laminate from the inner side flush with external surface in the middle of the span length, TC3, dedicated to $\boldsymbol{T}_{IS}$ in the stagnation point and positioned in the middle of the span length, TC4, dedicated to $\boldsymbol{T}_{WALL}$ and positioned at the front spar in the middle of the span length, TC5 and TC8, dedicated to $\boldsymbol{T}_{HE\_OUT}$ and $\boldsymbol{T}_{HE\_IN}$ respectively, TC6 and TC7, dedicated to $\boldsymbol{T}_{IS-TOP}$ and $\boldsymbol{T}_{IS-BOTTOM}$ respectively. An 8 channels acquisition system type NI-USB6210 was used to acquire

Figure 8: Prototype EHCLE1 assembled within IFF test chamber

the 8 thermocouples and it was powered and controlled through a USB connector to a laptop. Acquisition sampling was set to 2.0 [points/s]. A 450[W] DC power supply unit model ATE36-15M has been used to feed the EHCLE1 system with max current limited at 15[A] and max voltage limited at 36[V]. Accuracy of measured voltage as declared by the manufacturer is ± 0.1 [V] whilst the accuracy of the measured current is 0.01[A].

4 Experimental methodology and test results

The test campaign has been focused primarily to evaluate the thermal anti-icing performance of the system and therefore all tests have been performed at zero angle of attack. A thermal endurance test at RT has been also performed on the coupon to evaluate the interaction composite-resistance after cyclical thermal stress. The coupon has been cut in slices after TET for micrographic inspection and results compared to unstressed samples.

4.1 Test Facility

The test campaign has been performed using the IFF available at Department of Aerospace Engineering of the University of Naples Federico II, which has been equipped with a subsonic 120[mm] span, 300[mm] height and 400 [mm] long test

chamber. For the IFF functional principle see Russo et alii, 2009.

Icing Test Condition	Stagnation chamber	Water Spraying System		Test Chamber Flow		
	T_0	Air Pressure	Water Pressure	MVD	LWC	Mach Number
	[°C]	[bar]	[bar]	[μm]	[g m^{-3}]	-
ITC1	-20	0,60	0,20	35	0,3	0,2
ITC2	-20	0,60	0,30	35	0,4	0,2
ITC3	-20	0,60	0,40	50	0,7	0,2
ITC4	-20	0,70	0,20	30	0,2	0,2
ITC5	**-20**	**0,80**	**0,40**	**35**	**0,6**	**0,2**
ITC6	-10	0,80	0,60	50	1,0	0,2
ITC7	-10	0,90	0,10	25	0,2	0,2
ITC8	-10	0,90	0,40	30	0,5	0,2
ITC9	-10	1,00	0,10	20	0,1	0,2
ITC10	-10	1,00	0,60	35	0,8	0,2

Table 3: IFF calibrated Icing Test Conditions

The useful duration of a RUN is in the range of 4 to 5 [min] pending on the ambient temperature. Due to nature of the IFF facility for each value of $\boldsymbol{T}_0$ there is a correspondent and unique value of the Mach number driven by the pressure $\boldsymbol{P}_0$ in the stagnation chamber and the IFF components areal ratios. Since the water content makes the temperature in the stagnation chamber to decrease a calibration of the IFF was performed (see Tab. 3). Two temperatures, -10 and -20[˚C], have been calibrated showing that the top performance of the IFF is reached at -20[˚C], LWC=0.6 [g m^{-3}] and MVD of 35[μm] (see ITC5 in Tab. 3). LWC and MVD measurements were made using a Phase Doppler Particle Analyzer system.

4.2 Icing Test Matrix

The icing test Matrix was planned with the aim of scanning a wide range of supplied energies $\boldsymbol{Q}_J$ and monitoring the consequent thermal behaviour of the EHCLE laminate. A total of 78 runs have been performed including setup tests, aborted tests and tests with anomalies which have been repeated. In Tab. 4 only 35 significant runs are reported. Significant test have been repeated 3 times to evaluate the repeatability of the results. It is important to point out that due to limitation imposed by the IFF in terms of RUN duration it was possible but very tight to run icing tests with variable power densities and therefore a single value of $\boldsymbol{Q}_J$ per RUN was tested.

RUN ID	ITC	Functional Mode	Q_J [kW/m^2]	T_{ES} [°C]	Description
EHCLE1-IFF-RUN-1	ITC5 (LWC=0)	FM13	5,1	11,0	DRY−HTC calculation
EHCLE1-IFF-RUN-2	ITC5 (LWC=0)	FM14	9,6	39,9	DRY−HTC calculation
EHCLE1-IFF-RUN-3	ITC5 (LWC=0)	FM15	15,5	70,0	DRY−HTC calculation
EHCLE1-IFF-RUN-4	ITC5 (LWC=0)	FM13	5,2	12,0	DRY−HTC calculation−Repeatibility
EHCLE1-IFF-RUN-5	ITC5 (LWC=0)	FM14	9,5	40,3	DRY−HTC calculation−Repeatibility
EHCLE1-IFF-RUN-6	ITC5 (LWC=0)	FM15	15,5	69,0	DRY−HTC calculation−Repeatibility
EHCLE1-IFF-RUN-7	ITC5 (LWC=0)	FM13	5,0	10,0	DRY−HTC calculation−Repeatibility
EHCLE1-IFF-RUN-8	ITC5 (LWC=0)	FM14	9,5	41,2	DRY−HTC calculation−Repeatibility
EHCLE1-IFF-RUN-9	ITC5 (LWC=0)	FM15	15,3	72,0	DRY−HTC calculation−Repeatibility
EHCLE1-IFF-RUN-10	ITC5	Tentative	1,1	-14,3	Insufficient for Running Wet
EHCLE1-IFF-RUN-11	ITC5	Tentative	2,0	-10,5	Insufficient for Running Wet
EHCLE1-IFF-RUN-12	ITC5	Tentative	3,3	-4,6	Insufficient for Running Wet
EHCLE1-IFF-RUN-13	ITC5	Tentative	4,1	1,2	Insufficient for Running Wet
EHCLE1-IFF-RUN-14	ITC5	Tentative	5,3	6,9	Insufficient for Running Wet
EHCLE1-IFF-RUN-15	ITC5	Tentative	5,7	8,1	Insufficient for Running Wet
EHCLE1-IFF-RUN-16	ITC5	Tentative	6,1	8,9	Insufficient for Running Wet
EHCLE1-IFF-RUN-17	ITC5	Tentative	6,1	9,3	Insufficient for Running Wet / Repeatibility
EHCLE1-IFF-RUN-18	ITC5	FM12	6,5	9,9	Running Wet
EHCLE1-IFF-RUN-19	ITC5	FM12	6,5	10,5	Running Wet / Repeatibility
EHCLE1-IFF-RUN-20	ITC5	FM12	6,5	10,4	Running Wet / Repeatibility
EHCLE1-IFF-RUN-21	ITC5	FM11	8,6	12,2	Running Wet / Insuffcient for Full Evaporation
EHCLE1-IFF-RUN-22	ITC5	FM10	11,5	16,5	Running Wet / Insuffcient for Full Evaporation
EHCLE1-IFF-RUN-23	ITC5	FM9	12,9	20,1	Running Wet / Insuffcient for Full Evaporation
EHCLE1-IFF-RUN-24	ITC5	FM8	14,4	23,9	Running Wet / Insuffcient for Full Evaporation
EHCLE1-IFF-RUN-25	ITC5	FM7	16,0	28,9	Running Wet / Insuffcient for Full Evaporation
EHCLE1-IFF-RUN-26	ITC5	FM6	17,5	33,6	Running Wet / Insuffcient for Full Evaporation
EHCLE1-IFF-RUN-27	ITC5	FM5	19,3	39,2	Running Wet / Insuffcient for Full Evaporation
EHCLE1-IFF-RUN-28	ITC5	FM4	21,1	45,5	Running Wet / Insuffcient for Full Evaporation
EHCLE1-IFF-RUN-29	ITC5	FM3	23,0	52,6	Running Wet / Insuffcient for Full Evaporation
EHCLE1-IFF-RUN-30	ITC5	FM2	25,0	60,0	Running Wet / Insuffcient for Full Evaporation
EHCLE1-IFF-RUN-31	ITC5	FM16	26,2	66,2	Running Wet / Insuffcient for Full Evaporation
EHCLE1-IFF-RUN-32	ITC5	FM1	27,0	69,5	Fully Evaporative
EHCLE1-IFF-RUN-33	ITC5	FM1	27,1	70,5	Fully Evaporative / Repeatibility
EHCLE1-IFF-RUN-34	ITC5	FM1	27,0	72,1	Fully Evaporative / Repeatibility
EHCLE1-IFF-RUN-35	ITC5	FM17	30,0	77,0	Fully Evaporative / Overheating

Table 4: EHCLE Icing Test Matrix

4.3 Icing test method and uncertainty analysis

The icing test campaign has been performed under fixed icing condition as defined by the ITC5 in Tab.3. Majority of test were performed in winter to maximize the duration of the runs and the temperature of the model was always kept at -18 [°C] before run starting. Once the temperature $\boldsymbol{T}_{ES}$ measured on the model was stable at -20 [°C] the thermal test was started activating the power supply unit and the water spraying system. After the target power density $\boldsymbol{Q}_J$ was achieved the external surface temperature reached a new equilibrium value $\boldsymbol{T}_{ES}$ within a certain delay. Once at equilibrium the RUN was considered finished. The uncertainty analysis concern-

ing the temperature measurement is proposed assuming a linear combination of all single contributions. It accounts mainly for the position accuracy of the thermocouples estimated in about ± 2 [°C], the data acquisition system overall accuracy estimated in about ± 0.5 [°C], the thermocouple accuracy itself as declared by the manufacturer ± 1 [°C] and the electromagnetic interference intensity estimated in about ± 0.5 [°C]. As a result of this analysis the temperature measurements are affected by an overall accuracy of ± 4 [°C] for the power densities ranging 10 to 30 [kW m^{-2}] and slightly smaller for lower power densities.

4.4 Preliminary dry tests

Dry test were performed to check the functionality of components and instrumentation and to measure the effective convection coefficient $\boldsymbol{h}_{CDRY}$ on the external surface for various values of $\boldsymbol{T}_{ES}$. Within these tests, the surface temperature $\boldsymbol{T}_{ES}$ for the RW and FE cases was reproduced under dry conditions by using a reduced power $\boldsymbol{Q}_J$ as shown in Tab. 4. The coefficient $\boldsymbol{h}_{CDRY}$ measured in the stagnation point has been found constantly higher than the one measured at top and bottom extremities of the protected area.

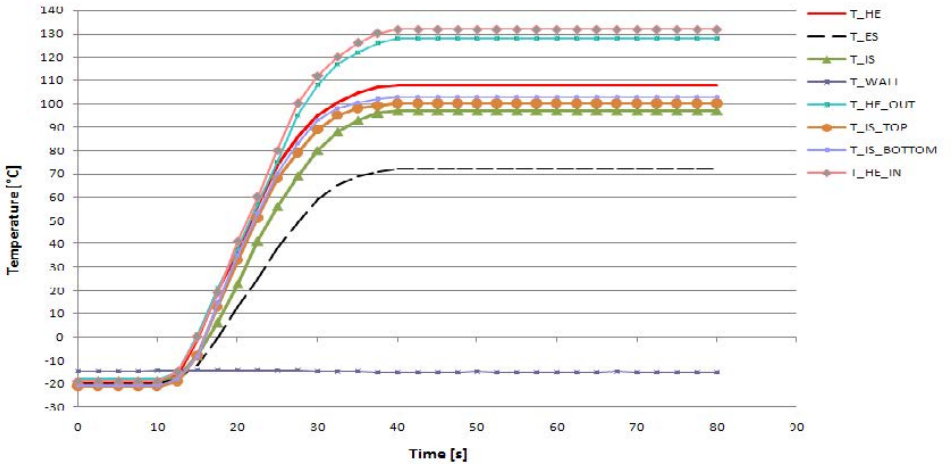

Figure 9: Typical dry run temperature plot (EHCLE1-IFF-RUN-9)

This is consistent with the fact that in the stagnation point the body can be approximated to a cylinder and therefore the heat exchanged is higher than the top and bottom extremities where the body can be approximated to a flat plate at small incidence. It is also important to point out that within the analytical model $\boldsymbol{h}_{CDRY}$ is calculated as an average over the whole heated area $\boldsymbol{A}_D$ considered as a cylinder

and therefore it is constant all along the heated area.

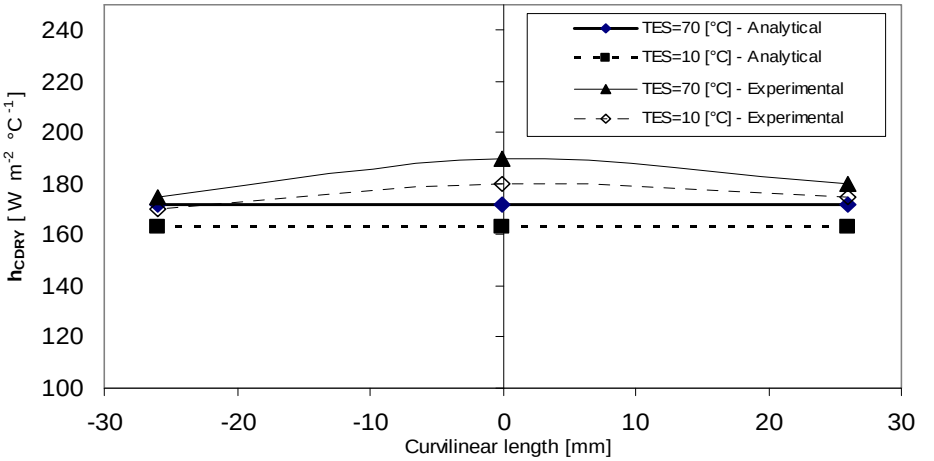

Figure 10: Analytical and experimental dry convection coefficients

4.5 Preliminary Icing tests

Preliminary Icing tests have been performed to evaluate ice shapes and the ice accretion mechanism. Preliminary Icing tests showed regular ice shapes following the leading edge profile with constant tendency to form a single horn on the top surface. Ice type was observed to be mixed type with a tendency to start accretion as rime type and continuing as mixed type with prevailing glaze appearance on top and bottom ice shape extremities. Ice accretion rate was measured resulting in an average value $\boldsymbol{M}_A = 0.025$ [g s^{-1}] with highest thickness ranging 6 to 10[mm] in the zone on top of the stagnation point and lowest thickness ranging 1 to 2[mm] in the area at top and bottom limits of the heated area.

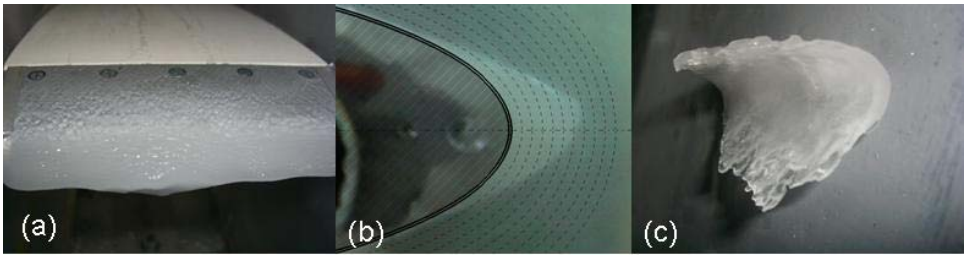

Figure 11: Typical ice shape: (a) front view, (b) side view, (c) detached

4.6 Preliminary tests with insufficient power for "Running Wet"

When $\boldsymbol{T}_{ES}$ was below 0 [˚C], continuous ice accretion was observed all over the leading edge, with an accretion peak around the stagnation point and some accretion reduction at top and bottom limits. At these locations the reduced accretion was quite irregular and difficult to quantify in relation to the supplied power density.

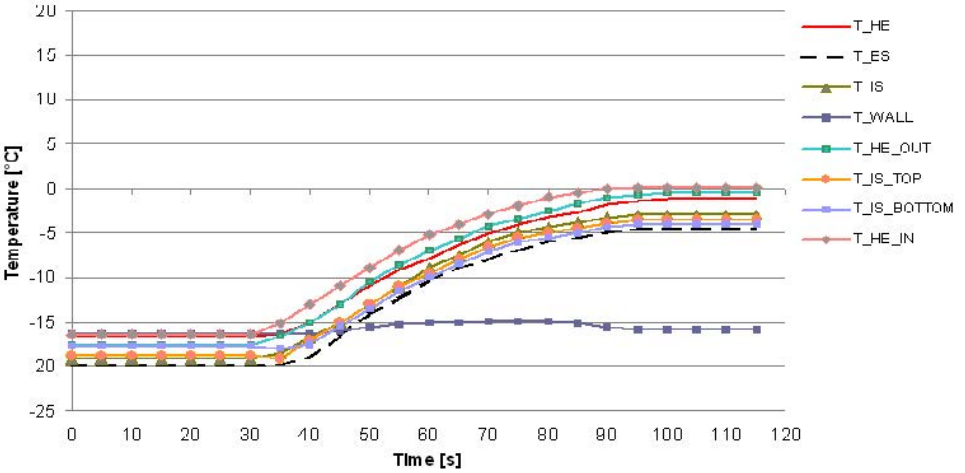

Figure 12: Typical temperature plot with T_{ES}<0[˚C] (EHCLE1-IFF-RUN-12)

When $\boldsymbol{T}_{ES}$ was above 0 [˚C], temporary ice accretion was observed but it was cyclically wiped away by the stream. This shows that the power required for a RW functional mode could be reduced increasing the power density only in the stagnation point area, reducing it at top and bottom limits of the heated area. A consistent amount of runback ice was observed for this type of tests. It is interesting to point out that the temperatures $\boldsymbol{T}_{IS}$ measured during the tests with insufficient power for running wet differ from top to bottom and both are lower than the $\boldsymbol{T}_{IS}$ measured behind the stagnation point. The higher values measured behind the stagnation point are consequence of a higher temperature of the external surface in the stagnation point. This is due to the fact that the ice was accreting at stagnation point first and then all along the leading edge offering a local shield to the leading edge itself which could not exchange heat anymore with a consequent increase of temperature behind the ice shape. This effect is reduced as the power approached that required for a RW system.

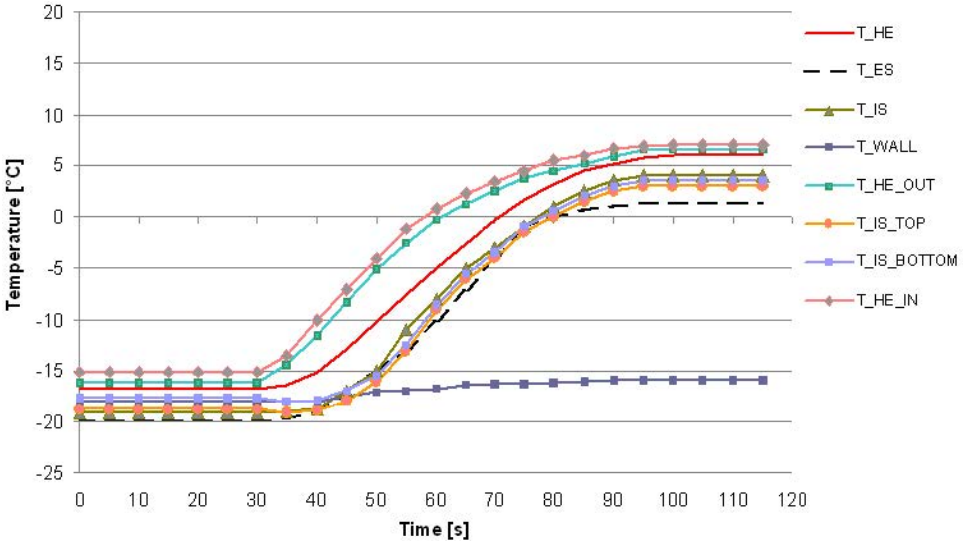

Figure 13: Typical temperature plot with T_{ES}>0[˚C] (EHCLE1-IFF-RUN-13)

4.7 Running Wet Tests

When T_{ES} was approaching 10[˚C], the cyclic phenomena previously described was vanishing, no ice accretion was observed on the leading edge and liquid water was flowing over the leading edge quite visibly. In these conditions we could assess that the "Running Wet" functional mode was achieved. This type of test was characterized by a power density of around 6.5 [kW m^{-2}] and runback ice downstream of the heated zone.

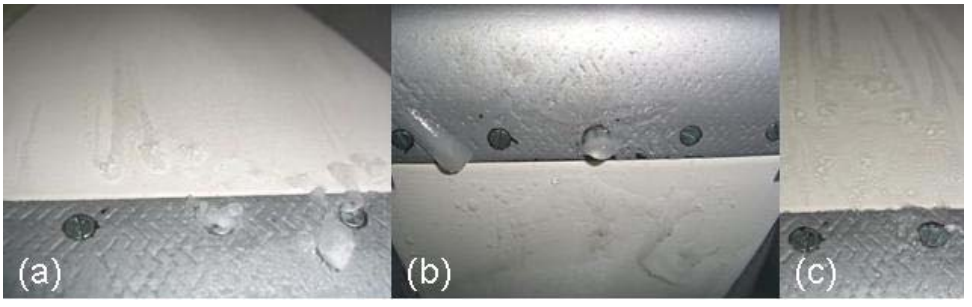

Figure 14: Runback ice after a RW run: top (a)(c) and bottom surfaces (b)

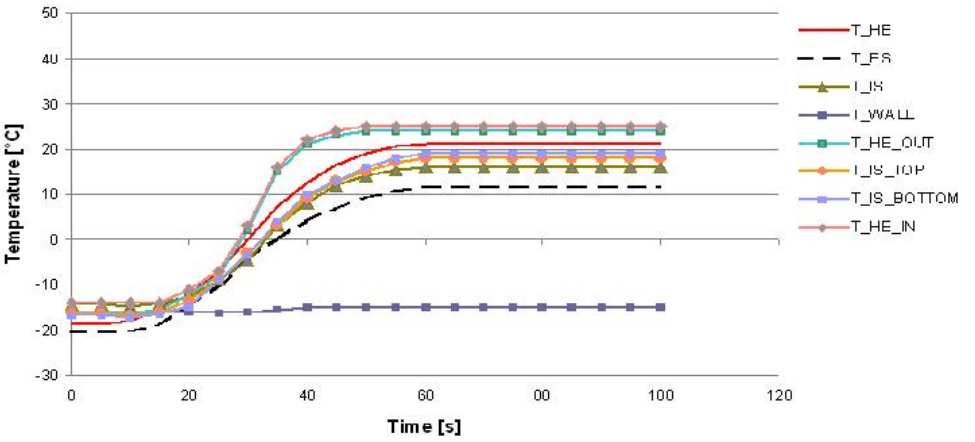

Figure 15: Typical temperature plot for RW case (EHCLE1-IFF-RUN-20)

4.8 Tests with insufficient power for "Full Evaporation"

When the power density $\boldsymbol{Q}_J$ was set from 6.5[kW m^{-2}] to approximately 26.0[kW m^{-2}], liquid water was observed to slip over the leading edge surface and always less runback ice was observed to accrete downstream the heated zone.

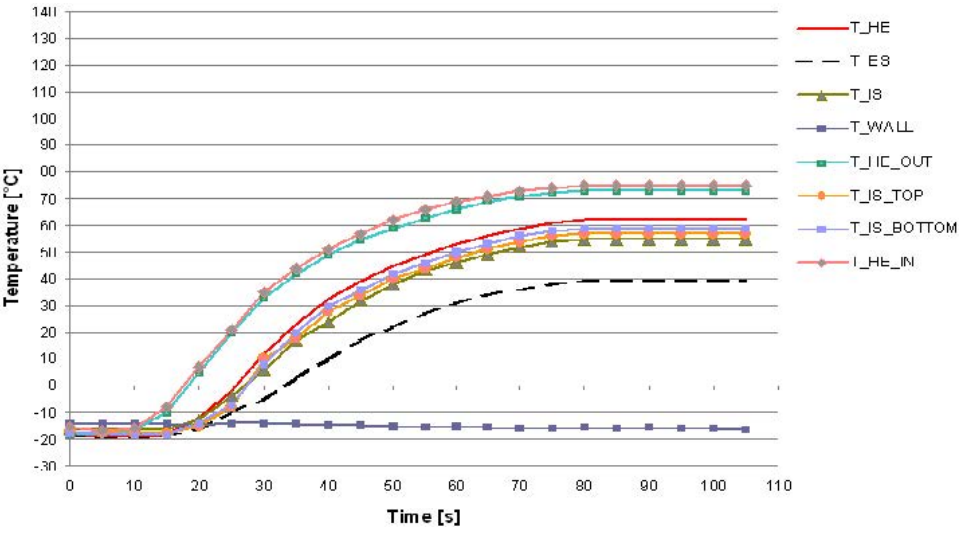

Figure 16: Typical temperature plot for non-FE case (EHCLE1-IFF-RUN-27)

4.9 Fully Evaporative tests

Approaching the power density $\boldsymbol{Q}_J$ of 27.0[kW m^{-2}], $\boldsymbol{T}_{ES}$ was topping 70[˚C], no trace of runback ice was observed downstream the heated zone and the liquid water previously observed to slip on the leading edge was barely visible.

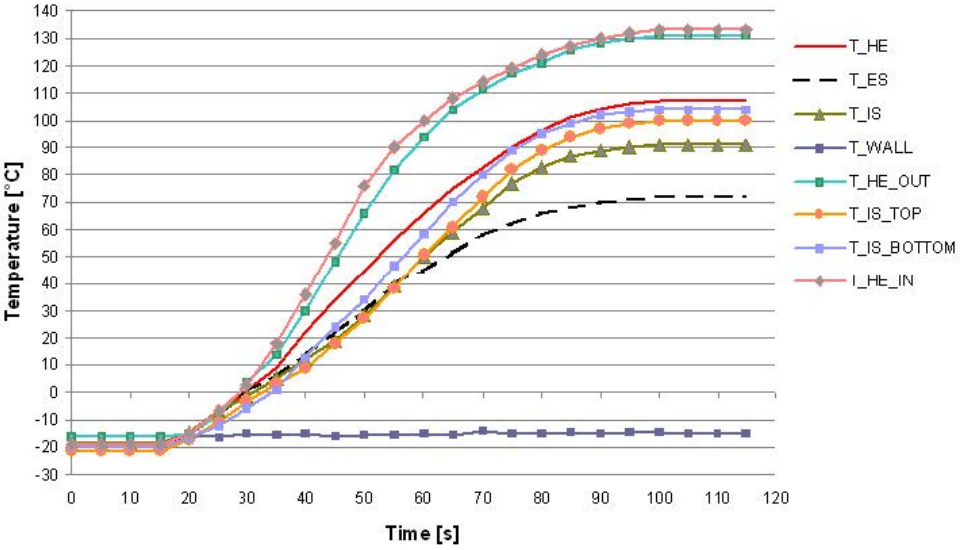

Figure 17: Typical temperature plot for FE case (EHCLE1-IFF-RUN-34)

In these conditions we could assess that the FE functional mode was achieved. A final test was performed at a power density of 30.0[kW m^{-2}] with similar results, $\boldsymbol{T}_{ES}$ rose almost up to 80[˚C] and no anomalies were reported.

4.10 Thermal Endurance Test (TET)

The Thermal Endurance Test was performed at RT which ranged from 12 to 20 [˚C], in an uncontrolled atmosphere (static air) and relative humidity ranging 50 to 60%. Temperature cycle evolution within days was monitored minimum once a day and is summarized in Fig. 19. The test has been running for 10^4 cycles with an average of 250 cycles per day for about two months.

After the TET the EHCLE coupon was cut in span and chord directions, examined through micrographic inspection and results compared to micrographic inspections of unstressed samples 5 to 7 (see Fig. 20). The micrographic inspection showed no matrix degradation by comparison to the unstressed samples, no delaminations

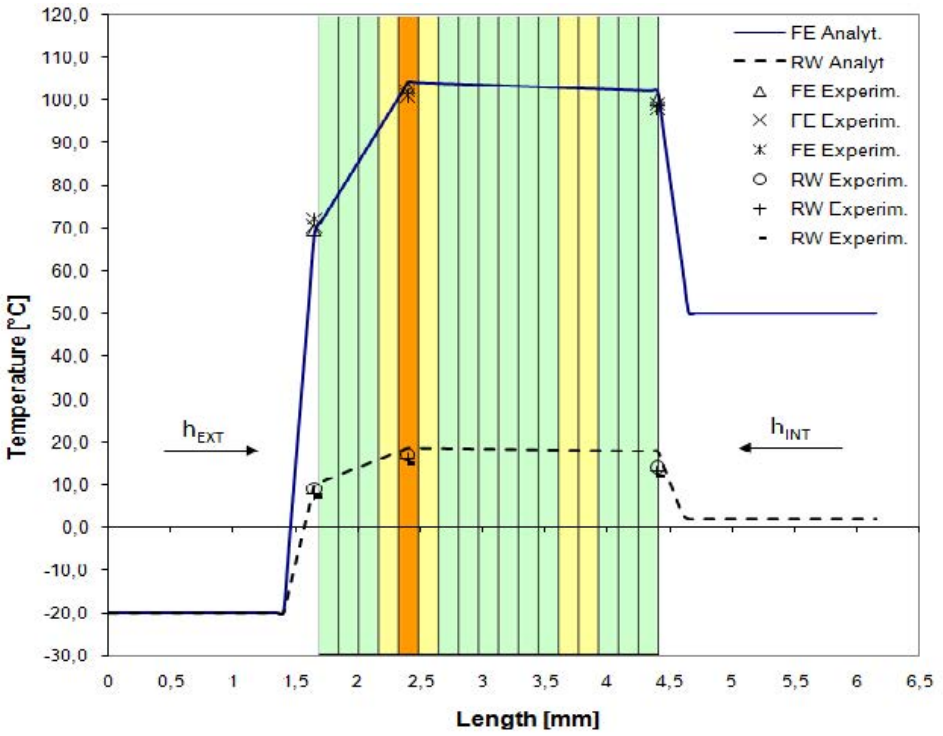

Figure 18: Analytical and experimental results for the RW and FE cases

and/or crack in the laminate and no degradation of the bond between heating element and fiberglass ply.

5 Conclusions

An investigation was conducted to evaluate the feasibility and the performance of an electrically heated composite leading edge for aircraft anti-icing applications. A prototype was designed, manufactured and equipped with an HT hybrid carbon-glass composite leading edge with embedded Ni alloy resistance. The average power densities supplied to the leading edge were ranging 1.0 to 30.0 [kW m^{-2}]. Thermal tests were performed under fixed icing conditions with zero angle of attack, Mach=0.2, total temperature -20[°C], LWC=0.6[g m^{-3}] and average MVD=35[μm]. A mixed ice accretion type was observed and "Running Wet" and "Fully Evaporative" functional modes were experimentally experienced at 6.5[kW m^{-2}] and 27.0[kW m^{-2}] respectively, in reasonable agreement with analytical forecast. In fully evaporative mode the max temperature recorded within the laminate

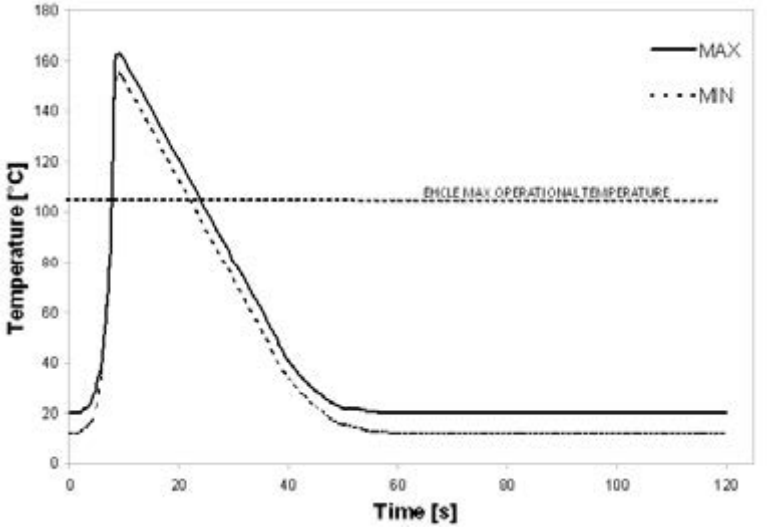

Figure 19: Thermal Endurance Test, load cycle envelope

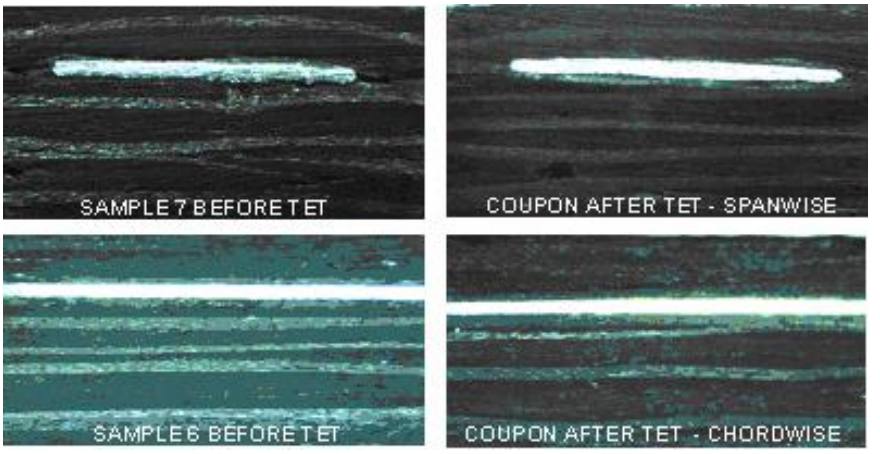

Figure 20: Micrographic Inspection before and after the TET

was 110[˚C]. A room temperature thermal endurance test has been run using a flat coupon fully representative of the leading edge laminate, for 10^4 cycles of 120[s] duration each, with peak temperatures ranging 155 to 165[˚C]. Micrographic inspection of the endurance coupon showed no evidence of laminate degradation in comparison to the unstressed laminate. The achieved results showed the great potentialities of the Electrical Heated Composite Leading Edge (EHCLE) which has

been constantly working below 60% of its maximum operative temperatures under the given icing conditions and the explored power densities. This potentiality justifies the need for future development in a larger scale under more severe icing conditions for a final assessment about both limit capabilities and applicability of such Icing Protection System to real aircraft.

References

Bragg M.B., Basar T., Perkins W.R., Selig M.S., Voulgaris P.G., Melody J.W., Sarter N.B. (2002): Smart icing systems for aircraft icing safety, *AIAA*, p. 0813.

Botura G.C., Sweet D. (2006): Concept Development of Low Power Electrothermal De-icing System. *AIAA*, p. 864.

Cenghel Y.A. (2003): Heat Transfer. A Practical Approach, *McGraw-Hill*.

Henry R. (1992): Development of an Electrothermal De-Icing/Anti-Icing Model. *AIAA*, p. 0526.

Ross H.A., Zumwalt R., Provose G., Padmanabhan J. , Thomson V., Riley, J. (1991): FAA Icing Handbook. *DOT/FAA/CT-88/8-2*.

Russo G.P., Esposito A., Esposito B., Renis R., De Rosa F., Parente F. (2010): Icing Tests in a Small Blow-Down Wind Tunnel. *FDMP: Fluid Dynamics & Materials Processing*, vol.6, no.3, pp. 319-335.